Sensorless DTC of Induction Motor Drive based on Full Order Extended Kalman Filter Observer

DJAMILA CHERIFI, YAHIA MILOUD
Department of Electrical
Engineering University of
Dr.Tahar Moulay
P. O. B. 138, 20000 Ennasr, Saida
ALGERIA

Abstract: - The induction motor is by far the most popular motor in the industry because of its benefits, which include low cost, ease of design and maintenance, and most importantly, the lack of a brush-collector assembly. However, high-performance power semiconductors, which make up the static converters connected to the control systems, have made it feasible to design systems that use induction motors running at varying frequencies. A new frontier in control was made possible by the introduction of direct torque control (DTC) in the middle of the 1980s. Direct torque management for an induction motor without a mechanical speed sensor is the primary focus of the work reported in this paper. Control strategies without mechanical sensors aim to develop high-performance drives, by freeing themselves from direct measurement of speed or position, which is then replaced by a calculation algorithm to reconstruct the motor speed from measurable electrical quantities. This work focuses on leveraging the high-gain Kalman filter observer to create an IM speed observation algorithm driven by a voltage inverter. After the endeavor, we will give simulation results to demonstrate the effectiveness of this approach.

Key-Words: - direct torque control, induction motor (IM), two-level voltage inverter, sensorless control, robust speed controller, Kalman filter, full-order observer.

Received: June 19, 2024. Revised: December 8, 2024. Accepted: December 28, 2024. Published: December 31, 2024.

1 Introduction

Variable speed has become a desired feature in all industrial areas. The recent development of variable speed drives has led to the gradual replacement of direct current machines by alternating current machines connected to static converters, [1], [2].

Induction motors are desirable in many industrial applications due to their durability, low cost, performance, and ease of maintenance. The advancement of power electronics and digital electronics now enables variable speed axis control in low-power applications, [3]. With the introduction of quick-switching components and the advancement of digital control technology, it is now possible to use a considerably more complex control structure. Thus, we may highlight control concepts that can achieve performance levels comparable to those of direct current machines, [4], [5].

Currently, AC machines' speeds are controlled via scalar or vector controllers. In these approaches, control algorithms are based on a model of the machine to be controlled, with the inverter acting as a voltage source that does not change them. Numerous studies have been conducted on scalar and vector controllers, resulting in a wide range of industrial applications, [6], [7], [8], [9]. To avoid the problems of sensitivity to parametric variations experienced by vector control, other control methods have been considered in which the flux and electromagnetic torque are estimated from the only electrical quantities accessible to the stator, and this is without the use of mechanical sensors. Among these methods, the direct torque control, based on the orientation of the stator flux and which was introduced in 1985 by [10] and [11].

Machine control requires accurate information from the processes under control in order to function properly. This information can originate from electrical or mechanical sensors, the latter of which are expensive and brittle, weakening electrical drive systems, [12], [13]. To address this issue, we choose a control without a mechanical sensor that is based on the design of a software sensor for the estimation of variables inaccessible to measurement or whose measurement requires relatively expensive sensors compared to the objective of the envisaged application, such as rotation speed, [14], [15], [16].

This paper describes the implementation of a method for measuring the speed of an IM powered by a voltage inverter using a high-gain Kalman filter observer. We conclude this research with simulation results that demonstrate the performance of this strategy.

2 Induction Motor Model and the Principle of the DTC

A dynamic model of the induction motor in the stator coordinates frame can be expressed by [17]:

$$\frac{di_{s\alpha}}{dt} = -\lambda i_{s\alpha} - \omega_r i_{s\beta} + \frac{R_s}{\sigma L_s L_r}\phi_{s\alpha} + \frac{\omega_r}{\sigma L_r}\phi_{s\beta} + \frac{1}{\sigma L_s}u_{s\alpha}$$

$$\frac{di_{s\beta}}{dt} = -\lambda i_{s\beta} + \omega_r i_{s\alpha} + \frac{R_s}{\sigma L_s L_r}\phi_{s\beta} - \frac{\omega_r}{\sigma L_r}\phi_{s\alpha} + \frac{1}{\sigma L_s}u_{s\beta}$$

$$\frac{d\phi_{s\alpha}}{dt} = u_{s\alpha} - R_s i_{s\alpha}$$

$$\frac{d\phi_{s\beta}}{dt} = u_{s\beta} - R_s i_{s\beta} \quad (1)$$

with $\lambda = \frac{R_s}{\sigma L_s} + \frac{R_r}{\sigma L_r}$

The torque equation is:

$$T_{em} = p\left(\phi_{s\alpha} i_{s\beta} - \phi_{s\beta} i_{s\alpha}\right) \quad (2)$$

The mechanical relationship is given by:

$$J\frac{d\Omega}{dt} = T_{em} - T_L - f\Omega \quad (3)$$

Vector expression of the voltage delivered by the voltage inverter is:

$$\vec{V}_s = \sqrt{\frac{2}{3}}\mathrm{V_{dc}}\left[S_a + S_b e^{j\frac{2\pi}{3}} + S_c e^{j\frac{4\pi}{3}}\right] \quad (4)$$

V_{dc} : represents the direct voltage.

The combination of the different states of the inverter gives 2^3=8 possible cases for the voltage vector V including two zero vectors (V_0 and V_7) and six non-zero vectors. Figure 1 shows the representation in the complex plane of the 8 positions of the vector V generated by a two-level voltage inverter.

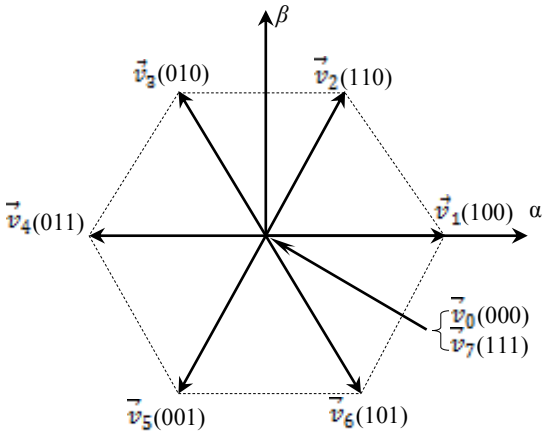

Fig. 1: Voltage vectors delivered by the two-level inverter

To achieve high control precision, DTC concentrates on adjusting torque and flux by choosing voltage vectors and keeping these two quantities in hysteresis bands, [18].

2.1 Stator Flux Estimation

According to the IM model, The stator flux is estimated by:

$$\hat{\phi}_s = \sqrt{\hat{\phi}_{s\alpha}{}^2 + \hat{\phi}_{s\beta}{}^2} \quad (5)$$

The two estimated flux components are:

$$\begin{cases} \hat{\phi}_{s\alpha} = \int_0^t (v_{s\alpha} - R_s i_{s\alpha})dt \\ \hat{\phi}_{s\beta} = \int_0^t (v_{s\beta} - R_s i_{s\beta})dt \end{cases} \quad (6)$$

with:

$$\angle\hat{\phi}_s = arctg\left(\frac{\hat{\phi}_{s\beta}}{\hat{\phi}_{s\alpha}}\right) \quad (7)$$

Figure 2 Diagram showing how the voltage model estimates the stator flux.

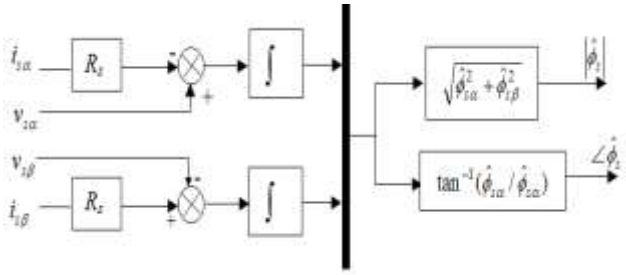

Fig. 2: Block diagram of stator flux estimation in (α, β) coordinates

2.2 Electromagnetic Torque Control

The general expression of electromagnetic torque is given by

$$T_{em} = p\frac{M}{\sigma L_s L_r}\phi_s.\phi_r Sin(\delta) \quad (8)$$

where:

p is the number of pole pairs.

ϕ_s, ϕ_r are stator and rotor flux vectors.

δ angle between the stator and rotor flux vectors

From expression (08), it is clear that the electromagnetic torque is controlled by the stator and rotor flux amplitudes. If those quantities are maintained constant, the torque can be controlled by adjusting the load angle δ.

- The torque is estimated by:

$$\hat{T}_{em} = p\left(\hat{\phi}_{s\alpha} i_{s\beta} - \hat{\phi}_{s\beta} i_{s\alpha}\right) \quad (9)$$

3 Development of Flux and Torque Controllers

3.1 Flux Hysteresis Controller

Its goal is to keep the flux vector's end in the circular ring depicted in Figure 3.

To choose the appropriate voltage vector, the corrector's output must show which way the flux module is evolving. A straightforward two-level hysteresis corrector is ideal for this and enables the achievement of excellent dynamic performances, [19].

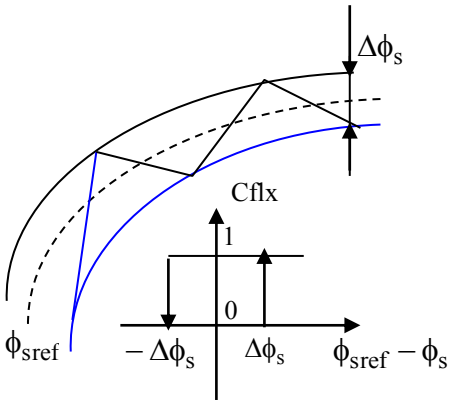

Fig. 3: Hysteresis flux corrector

3.2 The Torque Corrector

The torque corrector has the function of maintaining the torque within the limits $T_{em-ref} - T_{em} \le \Delta T_{em}$ with ΔT_{em} the torque reference to the hysteresis band of the corrector.

The structure of Three-level hysteresis controller is shown in Figure 4.

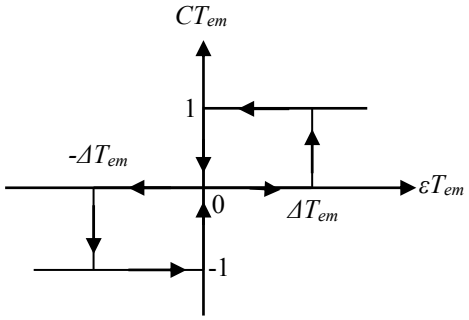

Fig. 4: Three-level hysteresis controller

It enables both positive and negative torque control over the motor in both rotational directions. The Boolean variable, which is the corrector's output, clearly shows whether the torque amplitude needs to be reduced (CT_{em} = 0) or increased in absolute value (CT_{em} = 1 for a positive setpoint and CT_{em} = -1 for a negative setpoint).

3.3 Development of Switching Tables

The control table is constructed according to the state of the variables Cflx and CT_{em}, and the position zone Z_i of ϕ_s . It is therefore presented in the following form, [20], [21]:

Table 1. DTC structure switching table

flux	Torque	zone "Z_i" 1	2	3	4	5	6	comparator
Cflx =1	CT_{em}=1	V_2	V_3	V_4	V_5	V_6	V_1	Two level
	CT_{em}=0	V_7	V_0	V_7	V_0	V_7	V_0	
	CT_{em}=-1	V_6	V_1	V_2	V_3	V_4	V_5	Three level
Cflx=0	CT_{em}=1	V_3	V_4	V_5	V_6	V_1	V_2	Two level
	CT_{em}=0	V_0	V_7	V_0	V_7	V_0	V_7	
	CT_{em}=-1	V_5	V_6	V_1	V_2	V_3	V_4	Three level

4 The Speed Control of the IM

It is commonly known that when the speed reference varies significantly (large overshoot of the speed response), asynchronous machines with PI correctors cannot achieve very excellent performances when their speed is regulated. In fact, the PI corrector encounters a considerable deviation when the speed reference varies significantly. This leads to a strong proportional action of the corrector, which causes the motor speed to overshoot, [22], [23]. The solution to this issue is to use an IP corrector in place of the PI (speed) corrector. Figure

5 shows the block diagram of an IP corrector.

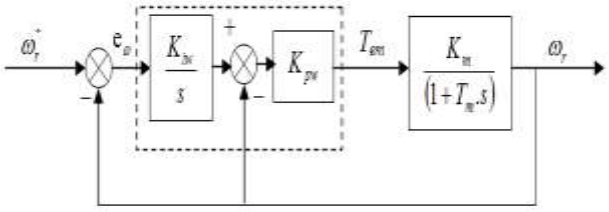

Fig. 5: An IP regulator-equipped external rotation speed control loop

In a closed loop, we obtain a transfer function of the form:

$$\frac{\omega_r}{\omega_r^*} = \frac{\dfrac{K_m.K_{i\omega}.K_{p\omega}}{T_m}}{s^2 + \dfrac{(1+K_m.K_{p\omega})}{T_m}s + \dfrac{K_m.K_{i\omega}.K_{p\omega}}{T_m}} \quad (10)$$

The IP corrector's parameters are obtained by imposing the poles in a closed loop:loop with an IP regulator, These parameters are cited in Table 2.

Table 2. The IP corrector's parameters

	$K_{p\omega}$	$K_{i\omega}$
Corrector IP	$(2\xi\omega_0 T_m - 1)/K_m$	$\omega_0{}^2 T_m / K_m K_{p\omega}$

5 Kalman Filter Observer

The existence of noise is one of several presumptions that make the Kalman filter a state observer. This observer's guiding principle is to minimize the variance of the estimation measurement error depending on the state, [24], [25].

The Kalman filter is expressed as:

$$\frac{d}{dt}x = Ax + Bu + U(t).w(t) \quad (11)$$

$$y = Cx + v(t) \quad (12)$$

with

$U(t)$ = weight matrix of noise

$v(t)$ = noise matrix of output model (measurement noise)

$w(t)$ = noise matrix of state model (system noise)

$U(t)$, $v(t)$, and $w(t)$ are assumed to be stationary, white, and Gaussian noise, and their expectation values are zero.

This noise's covariance matrices (Q) and (R) are described as:

$$Q = \text{convaiance}\ (w) = E\{ww'\} \quad (13)$$

$$R = \text{convaiance}\ (v) = E\{vv'\} \quad (14)$$

where $E\{.\}$ denotes the expected value.

The following is a schematization of the Kalman filter's general principle.

The configuration of the basic Kalman filter observer is illustrated in Figure 6.

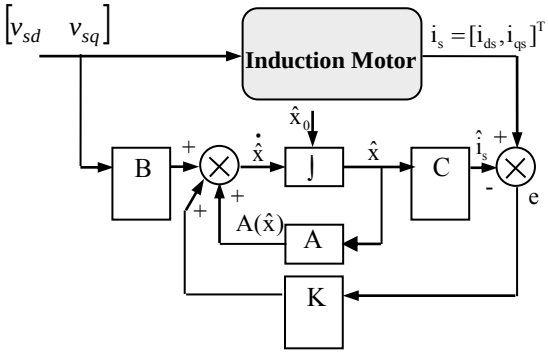

Fig. 6: The basic configuration of the Kalman filter observer

The Kalman filter equation of state is provided by:

$$\dot{\hat{x}} = (A - KC)\hat{x} + Bu + Ky \quad (15)$$

In the Kalman filter matrix, the noise covariance "K" is a fundamental component. The following is a gauge of the observation's quality:

$$L_x = \sum E\left\{[x(k) - (k)]^T [x(k) - \hat{x}(k)]\right\} = \min \quad (16)$$

The discrete steps of the Kalman filter are given by:

(1) Estimation step (system state)

$$x(k+1) = x(k) + K(k)(y(k) - \hat{y}(k)) \quad (17)$$

(2) Renew of the error covariance matrix

$$P(k+1) = P(k) - K(k)h^T(k+1)\,P(k) \quad (18)$$

(3) Calculation of Kalman filter gain matrix

$$K(k+1) = P^*(k+1)h^T(k+1)\left[h(k+1)P^*(k+1)h^T(k+1) + R\right]^{-1} \quad (19)$$

(4) Prediction of state matrix

$$f(k+1) = \frac{\partial}{\partial x}(A_d x + B_d v)\Big|_{x=\hat{x}(k+1)} \quad (20)$$

(5) Estimation of error covariance matrix

$$P^*(k+1) = f(k+1)\hat{P}(k)f^T(k+1) + Q \quad (21)$$

Discretization of (10) and (11) yields

$$x(k+1) = A_d(k)x(k) + B_d(k)u(k) \quad (22)$$

$$y(k) = C_d(k)x(k) \quad (23)$$

A stochastic state observer called the Kalman filter is used to jointly estimate the parameters and state of a nonlinear dynamical system, [26].

The discrete system's state and output are represented by x(k) and y(k), respectively, while the input and output matrices are represented by Ad, Bd, and Cd.

The IM's discrete model can be expressed as follows:

$$\begin{aligned} x(k+1) &= f(x(k),u(k)) + w(k) = A_d x(k) + B_d u(k) + w(k) \\ y(k) &= h(x(k)) + V(k) = C_d x(k) + V(k) \end{aligned} \quad (24)$$

with *w(k)* is the measurement noise and *V(k)* is the process noise.

The state vector is chosen to be:

$$\begin{aligned} A_d &= e^{AT_s} \approx I - AT_s \\ B_d &= \int_0^T e^{A\tau} Bd\tau \approx BT_s \\ C_d &= C \end{aligned} \quad (25)$$

6 Application of the Extended Kalman Filter to the MAS

6.1 State Model of the MAS in the (α,β) Frame

It is appropriate to employ an axis frame connected to the stator in order to implement the state equations of the machine model that will be used to create our observer. Consequently:

$$X = [i_{s\alpha} \quad i_{s\beta} \quad \phi_{s\alpha} \quad \phi_{s\beta}]^T ; U = [v_{s\alpha} \quad v_{s\beta}]^T$$

$$B = \begin{bmatrix} \frac{1}{\sigma L_s} & 0 \\ 0 & \frac{1}{\sigma L_s} \\ 0 & 0 \\ 0 & 0 \end{bmatrix};$$

The following format can be used to express the equations of state:

$$\begin{cases} \dot{i}_{s\alpha} = -\lambda i_{s\alpha} + \omega_r i_{s\beta} + \frac{K}{T_r}\phi_{s\alpha} + \omega_r . K\phi_{s\beta} + \frac{1}{\sigma L_s} v_{s\alpha} \\ \dot{i}_{s\beta} = -\omega_r i_{s\alpha} - \lambda i_{s\beta} - \omega_r . K\phi_{s\alpha} + \frac{K}{T_r}\phi_{s\beta} + \frac{1}{\sigma L_s} v_{s\beta} \\ \dot{\phi}_{s\alpha} = -R_s i_{s\alpha} \\ \dot{\phi}_{s\beta} = -R_s i_{s\beta} \end{cases} \quad (26)$$

where:

$$T_r = \frac{L_r}{R_r}; \; T_s = \frac{L_s}{R_s}; \quad K = \frac{1}{\sigma L_s}; \quad \lambda = \frac{1}{\sigma}\left(\frac{1}{T_r} + \frac{1}{T_s}\right)$$

5.2 The IM Extended State Model

We will utilize the model (1) acquired in section 2 to estimate the induction motor's speed. The machine's extended model in the reference frame connected to the stator is as follows:

$$f = \begin{bmatrix} -\lambda . x_1 + \omega_r . x_2 + \frac{K}{T_r} x_3 + K . \omega_r . x_4 + \frac{1}{\sigma L_s} v_{s\alpha} \\ -\omega_r . x_1 - \lambda . x_2 - K . \omega_r . x_3 + \frac{K}{T_r} . x_4 + \frac{1}{\sigma L_s} v_{s\beta} \\ -R_s x_1 \\ -R_s x_2 \\ 0 \end{bmatrix} \quad (27)$$

These are the stator states and voltages:

$$\begin{aligned} U &= \begin{bmatrix} v_{s\alpha} & v_{s\beta} \end{bmatrix}^T ; \\ X &= \begin{bmatrix} x_1 & x_2 & x_3 & x_4 & x_5 \end{bmatrix}^T \\ &= \begin{bmatrix} i_{s\alpha} & i_{s\beta} & \phi_{s\alpha} & \phi_{s\beta} & \omega_r \end{bmatrix}^T \end{aligned}$$

The following is the deduction of the Jacobian matrix "F":

$$F = \begin{bmatrix} 1 - t_e . \lambda & t_e . \omega_r & t_e . \frac{K}{T_r} & t_e . K . \omega_r & t_e . i_{s\beta} + t_e . K . \phi_{s\beta} \\ -t_e . \omega_r & 1 - t_e . \lambda & -t_e K . \omega_r & t_e . \frac{K}{T_r} & -t_e . i_{s\alpha} - t_e . K . \phi_{s\alpha} \\ -t_e . R_s & 0 & 0 & 0 & 0 \\ 0 & -t_e . R_s & 0 & 0 & 0 \\ 0 & 0 & 0 & 0 & 1 \end{bmatrix} \quad (28)$$

The matrix of measurements H is provided by:

$$H = \begin{bmatrix} 1 & 0 & 0 & 0 & 0 \\ 0 & 1 & 0 & 0 & 0 \end{bmatrix} \quad (29)$$

Selecting the appropriate values for the covariance matrices (Q) and (R) is a crucial and challenging step in the construction of the full-order EKF. Both the dynamic and steady-state states are impacted by changes in covariance matrix values.

The selected values for the covariance matrices (Q), (R), and (P) can be initialized and modified as follows to provide improved stability, convergence time, and significant speed of the EKF.

$$P = diag\left[1e^{-2} \quad 1e^{-2} \quad 1e^{-3} \quad 1e^{-3} \quad 15\right]$$

$$Q = diag\left[1e^{-6} \quad 1e^{-6} \quad 1e^{-3} \quad 1e^{-3} \quad 1e^{2}\right]$$

$$R = diag\left[1e^{2} \quad 1e^{2}\right]$$

7 Simulation Results and Discussion

Two scenarios were simulated in order to show how well the suggested estimation method worked when integrated into a DTC-controlled instant messaging speed modification system. These will be covered in the sections that follow.

The assessment of speed in the presence of load disturbances and rotational direction reversal,

Table 3 lists the specifications for the 1.5 kW three-phase squirrel cage motor.

Table 3. IM motor parameters

Item	Symbol	Data
IM Mechanical Power	P_W	1.5 Kw
Nominal speed	ω	1420 rpm
Nominal Frequency	f	50 Hz
Pole pairs number	P	2
Stator resistance	R_s	4.85Ω
Rotor resistance	R_r	3.805Ω
Stator self-inductance	L_s	274 mH
Rotor self-inductance	L_r	274 mH
Mutual inductance	L_m	258 mH
Moment of inertia	J	0.031 kg.m^2
Friction coefficient	F	0.00114kg.m^2/s

The block design for an induction motor's sensorless direct torque control with a full-order Kalman filter observer is displayed in Figure 7. The number of sensors utilized in this construction has been reduced by the employment of full-order observers.

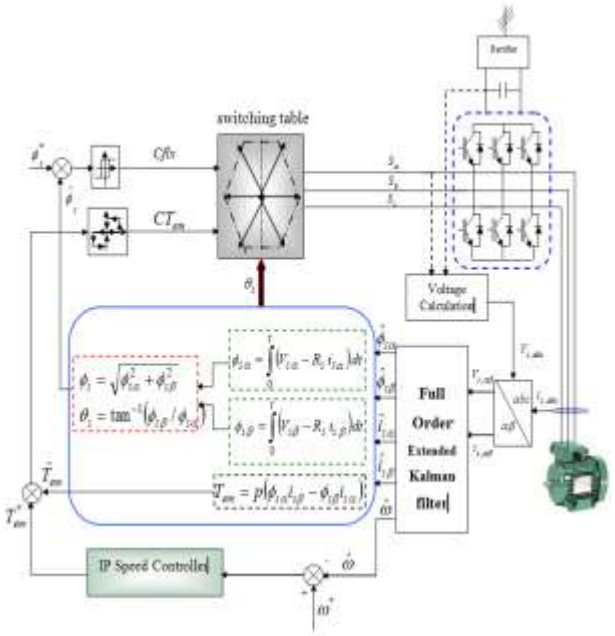

Fig. 7: Global induction motor sensorless DTC technique with full order extended Kalman filter observer is shown

7.1 Influence of Load Torque Variation

The system was simulated in this section with a speed setpoint of 150 rad/sec and a load torque of 10 Nm applied between t = 1s and t = 2s. Figure 8 shows the data we obtained.

With a very good rejection of load disturbance and no deformation, the simulation results demonstrate that the estimated speed precisely matches the reference. It is also observed that the estimation error is acceptable. Additionally, it is observed that the torque and flux are decoupled and that the stator flux is orientated correctly.

These findings demonstrate that the Kalman filter observer can be effectively used to directly adjust torque without a speed sensor in relation to load fluctuation.

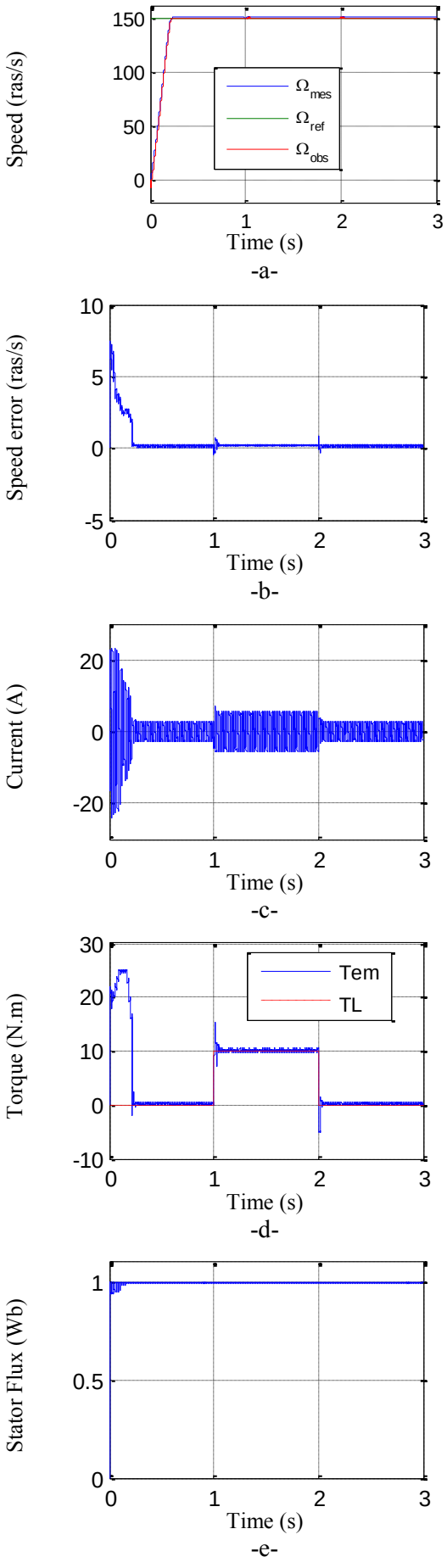

Fig. 8: Complete Order Sensorless DTC Command Responses Based on EFK Observers

7.2 Influence of the Reverse Direction of Rotation

We apply a shift of the speed setpoint from 150 rad/s to –150 rad/s from time t=3s, while applying a load torque of 10 N.m between periods t1 = 1s and t2 = 2s, respectively, to verify the resilience of the control method related to the FKE observer. Figure 9 shows the data we obtained. The following outcomes were attained by us:

We observe that the rotation speed estimation is nearly flawless. With nearly 0% static inaccuracy, the projected speed closely matches the real speed. We find a comparatively short rejection time and excellent sensitivity to load perturbations.

Additionally, we note that the stator flux is excellently oriented. The electromagnetic torque is affected by this. The flux's orientation is not

weakened by the torque's direction shift during the setpoint evolutions, especially during the rotation inversion. We also observe a good estimation of the stator currents and a flawless continuation of the estimated stator flux components to their corresponding real components.

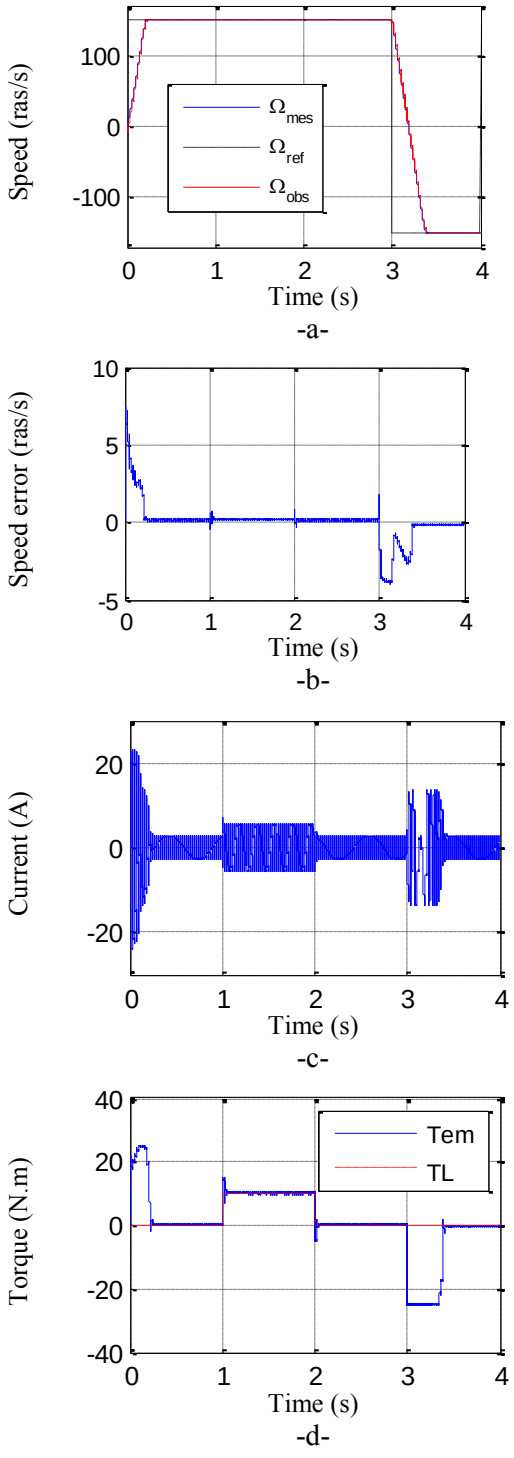

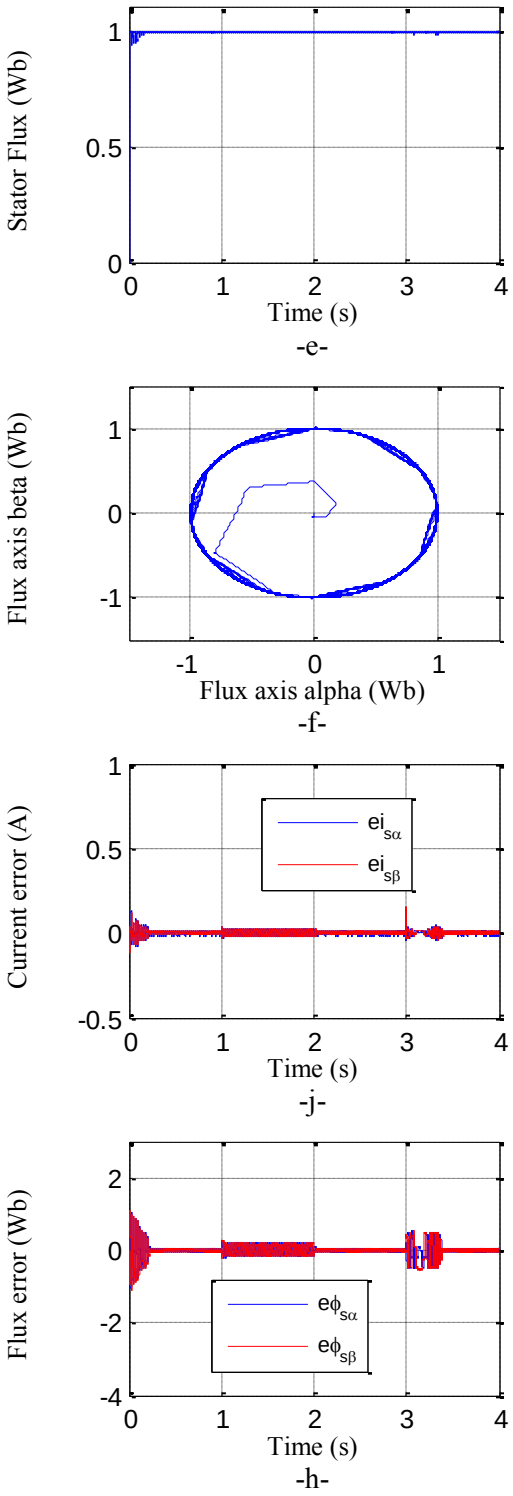

Fig. 9: Sensorless DTC control responses for load torque variation and rotational direction reversal based on Full Order EFK Observer

8 Conclusion

By eliminating the need for direct speed or position measurement and substituting it with a computation technique that reconstructs the motor speed from quantifiable electrical characteristics, mechanical

sensorless control schemes seek to provide high-performance drives.

Sensorless control of mechanical speed is developing. It seeks to do away with sensors' shortcomings, including their cost, noise, and fragility.

In this study, we used a full-order Kalman filter to examine the observer. This method was applied in the DTC to enhance the three-phase induction motor's sensorless control performance when connected to an IP controller.

The induction motor was initially introduced in this paper from a modeling and control perspective. By considering the simplifying assumptions, we were able to develop a mathematical model of the induction motor. By precisely maintaining the decoupling between the torque and the flux, the direct torque control approach enabled us to regulate the induction motor and so make it easier to regulate the machine speed.

When compared to the test of the controller with a classic PI structure, the IP controller provided better dynamic performance for the transient regime; decoupling was preserved, and the induction motor's response time and speed overshoot were significantly better with IP than with a classic PI.

It may be inferred from the simulation results that the suggested observation method is appropriate for all operational circumstances. The suggested observer (full-order Kalman filter), on the other hand, has good robustness with regard to the variation of the load and the pursuit, enabling good functional performance with a low-cost and reduced volume installation. This gives our control a minimal structure (elimination of all sensors: speed, currents, and flux), which supports the notion that this observer is robust.

References:

[1] S. A. Othman, J. A.-K Mohammed and F. M. Mohammed, "Variable Speed Drives in Electric Elevator Systems: A Review", *Journal of Physics: Conference Series,* 1973 (2021) 012028, doi: 10.1088/1742-6596/1973/1/012028..

[2] M.A. Hannan, Jamal A. Ali, Azah Mohamed, Aini Hussain, "Optimization techniques to enhance the performance of induction motor drives: A review", *Renewable and Sustainable Energy Reviews*, (2017), http://dx.doi.org/10.1016/j.rser.2017.05.240.

[3] Woosuk Sung, Jincheol Shin, and Yu-seok Jeong, " Energy-Efficient and Robust Control for High-Performance Induction Motor Drive With an Application in Electric Vehicles", *IEEE Transactions on Vehicular Technology,* vol. 61, No. 8, October 2012, doi: 10.1109/TVT.2012.2213283.

[4] R. R. Gomes, L. F. Pugliese, W.W. A. G. Silva, C. V. Sousa, G. M. Rezende and F. F. Rodor, "Speed Control with Indirect Field Orientation for Low Power Three-Phase Induction Machine with Squirrel Cage Rotor", *Machines,* 2021, 9, 320. https://doi.org/10.3390/machines9120320.

[5] M. U. Sardar, T. Vaimann, L. Kütt, A. Kallaste, B. Asad, S. Akbar and K. Kudelina, "Inverter-Fed Motor Drive System: A Systematic Analysis of Condition Monitoring and Practical Diagnostic Techniques", *Energies,* 2023, 16, 5628. https://doi.org/10.3390/en16155628.

[6] H. Mikhael D. Habbi, H. J. Ajeel, I. I. Ali, " Speed Control of Induction Motor using PI and V/F Scalar Vector Controllers", *International Journal of Computer Applications (0975–8887),* Vol. 151, No.7, October 2016, https://doi.org/10.5120/ijca2016911831.

[7] B. D. E. Cherif, A. Djerioui, S. Zeghlache, S. Seninete, A. Tamer, "Indirect vector controlled of an induction motor using H∞ current controller for IGBT open circuit fault compensation" *Int Trans. Electr. Energ. Syst.,* 2020;e12540. https://doi.org/10.1002/2050-7038.12540.

[8] Y. Zahraoui, M. Akherraz, C. Fahassa, S. Elbadaoui, " Induction motor harmonic reduction using space vector modulation algorithm", *Bulletin of Electrical Engineering and Informatics,* Vol. 9, No. 2, April 2020, pp. 452~465. DOI: 10.11591/eei.v9i2.1682.

[9] A. G. M. A. Aziz, Y. A. Almoataz, M. A. Ziad and A. A. Zaki Diab, "A Comprehensive Examination of Vector-Controlled Induction Motor Drive Techniques", *Energies*, 2023, 16, 2854. https://doi.org/10.3390/en16062854.

[10] Takahashi, I., Noguchi, T. (1986). A new quick response and high efficiency control strategy of an induction motor. *IEEE Trans. Ind. Applicat,* vol. IA-22, pp. 820-827. https://doi.org/10.1109/TIA.1986.4504799.

[11] Depenbrok, M. (1988). Direct self-control (DSC) of inverter fed induction machine. *IEEE Trans. Power Electron.,* vol. PE-3, pp. 420–429. https://doi.org/10.1109/63.17963.

[12] H. Mohan, M. K. Pathak & S. K. Dwivedi, " Sensorless Control of Electric Drives – ATechnological Review", *IETE Technical*

Review, 2019, https://doi.org/10.1080/02564602.2019.1662738.

[13] Krishna SM, Daya JL, Padmanaban FS, Mihet-Popa L (2017) Real-time analysis of a modified state observer for sensorless induction motor drive used in electric vehicle applications. *Energies,* 10(8):1077 https://doi.org/10.3390/en10081077.

[14] Kumar R, Das S, Bhaumik A (2019) Speed sensorless model predictive current control of doubly-fed induction machine drive using model reference adaptive system. *ISA Trans.,* 86:215–226 https://doi.org/10.1016/j.isatra.2018.10.025.

[15] Korzonek M, Tarchala G, Orlowska-Kowalska T (2019) A review on MRAS-type speed estimators for reliable and efficient induction motor drives. *ISA Trans.,* 93:1–13 https://doi.org/10.1016/j.isatra.2019.03.022.

[16] Ammar, A., Bourek, A., Benakcha, A. (2019). Robust load angle direct torque control with SVM for sensorless induction motor using sliding mode controller and observer. *Int. J. Computer Aided Engineering and Technology,* Vol. 11, No. 1, pp.14-34. https://doi.org/10.1504/IJCAET.2019.096713.

[17] D. Cherifi , Y. Miloud, "Contribution to the Improvement of Sensorless DTC-SVM for Three-Level NPC Inverter-fed Induction Motor Drive", *WSEAS Transactions on Power Systems,* Vol. 18, 2023. https://doi.org/10.37394/232016.2023.18.43.

[18] M. Said, D. Aziz, N. El Ouanjli, M. A Mossa, M. Sagar Bhaskar, K. L. Ngo, V. Q. Nguyen, " A New Robust Direct Torque Control Based on a Genetic Algorithm for a Doubly-Fed Induction Motor: Experimental Validation", *Energies,* 15, 5384. 2022, https://doi.org/10.3390/en15155384.

[19] M. Zaid Aihsan, A. Jidin, A. Alias, S. A. A. Tarusan, Z. Md Tahir, T. Sutikno, "Torque ripple minimization in direct torque control at low-speed operation using alternate switching technique", *International Journal of Power Electronics and Drive System (IJPEDS),* Vol. 13, No. 1, March 2022, pp. 631~642 https://doi.org/10.11591/ijpeds.v13.i1.pp631-642.

[20] A. Zemmit, S. Messalti, A. Harrag, "A new improved DTC of doubly fed induction machine using GA-based PI controller", *Ain Shams Engineering Journal*, Vol. 9, No. 1, pp. 1877–1885, 2018. https://doi.org/10.1016/j.asej.2016.10.011.

[21] M. El Mahfoud, B. Bossoufi , N. El Ouanjli , S. Mahfoud, M. Taoussi, "Three Speed Controllers of Direct Torque Control for a Doubly Fed Induction Motor Drive–A Comparison", *Electrica,* 2021; 21(1): 129-141 https://doi.org/10.5152/electrica.2021.20060.

[22] A. A. Zaki Diab, A. M. El-Sayed, H. Abbas, M. Abd El Sattar, "Robust Speed Controller Design Using H_infinity Theory for High-Performance Sensorless Induction Motor Drives". *Energies*, pp. 1-21, 2019.

[23] B. Moaveni, M. Khorshidi "Robust speed controller design for induction motors based on IFOC and Kharitonov theorem", *Turkish Journal of Electrical Engineering & Computer Sciences,* pp.1173–1186, 2015. https://doi.org/10.3906/elk-1306-22.

[24] D. Simon " Kalman Filtering with State Constraints: A Survey of Linear and Nonlinear Algorithms", *IET Control Theory and Applications,* 2009. doi: 10.1049/iet-cta.2009.0032.

[25] P. Tety, A. Konaté, O. Asseu, E. Soro, P. Yoboué, A. R. Kouadjo, "A Robust Extended Kalman Filter for Speed-Sensorless Control of a Linearized and Decoupled PMSM Drive", *Engineering,* 7(10), pp. 691–699, 2015. https://doi.org/10.4236/eng.2015.710060.

[26] D. Cherifi , Y. Miloud, " Improved Sensorless Control of Doubly Fed Induction Motor Drive Based on Full Order Extended Kalman Filter", *Periodica Polytechnica Electrical Engineering and Computer Science,* 64(1), pp. 64–73, 2020. https://doi.org/10.3311/PPee.14245.

Contribution of Individual Authors to the Creation of a Scientific Article (Ghostwriting Policy)

The authors equally contributed in the present research, at all stages from the formulation of the problem to the final findings and solution.

Sources of Funding for Research Presented in a Scientific Article or Scientific Article Itself

No funding was received for conducting this study.

Conflict of Interest

The authors have no conflicts of interest to declare.

Creative Commons Attribution License 4.0 (Attribution 4.0 International, CC BY 4.0)

This article is published under the terms of the Creative Commons Attribution License 4.0 https://creativecommons.org/licenses/by/4.0/deed.en_US